Sm^{3+}-Mn^{4+} activated Sr_2GdTaO_6 red phosphor for plant growth lighting and optical temperature sensing

Bingjie Han[1], Jiabao Zhu[1], Chu Chu[1], Xinghua Yang[1,*], Yuhan Wang[1], Kairan Li[1], Yuting Hou[1], Kang Li[2], Nigel Copner[2], Pingping Teng[1]

[1]Key Laboratory of In-Fiber Integrated Optics, Ministry of Education, College of Physics and Optoelectronic Engineering, Harbin Engineering University, Harbin 150001, China

[2]Wireless & Optoelectronics Research & Innovation Centre, Faculty of Computing, Engineering & Science, University of South Wales, Wales, CF37 1DL, UK

Fax: 0086-451-82519850

Phone: 0086-451-82519850

E-mail:*yangxh@hrbeu.edu.cn;

[1] Harbin Engineering University, College of Physics and Optoelectronic Engineering, Harbin 150001, P. R. China

***Abstract**:* Optical temperature sensing and plant growth lighting multifunctional applications can be realized by red luminescent materials. In this paper, novel Sm^{3+} and Sm^{3+}-Mn^{4+} activated Sr_2GdTaO_6 (SGTO) red phosphors for plant growth and optical temperature sensing were comprehensively analyzed. The phase, luminescence property and thermal stability of the material were tested. For PL performance, SGTO:0.075Sm^{3+} exhibits the maximum emission intensity in the range (560-670 nm). The emission range of SGTO:0.075Sm^{3+} after introducing Mn^{4+} is mainly dark red light emission in the range from 630 to 750 nm, and the optimum doping concentration of Mn^{4+} is determined to be 0.3%. The emission band of SGTO:0.075Sm^{3+} and SGTO:0.075Sm^{3+}, 0.003Mn^{4+} matches the absorption band of the plants. For optical temperature sensing properties, the relative sensitivity (S_r) and absolute sensitivity (S_a) of SGTO:0.075Sm^{3+}, 0.003Mn^{4+} are 2.94 K^{-1} (298 K) and 0.635 K^{-1} (573 K), respectively. The results indicate that Sm^{3+}-Mn^{4+} activated SGTO red phosphor is a luminescent material with potential application in plant growth and optical temperature sensing field.

***Key words**:* Phosphors; Double perovskite; Optical temperature sensing; Plant growth.

1 Introduction

Temperature detection has important applications in medical diagnostic, aerospace field, daily life, industrial production and agricultural science [1-8]. Therefore, the accuracy and ease of temperature assessment are the focus of current research in the scientific community. Non contact, low interference, real-time response, high resolution and non-invasive are the advantages of optical temperature sensing technology [9-14]. Fluorescence intensity ratio (FIR) technology avoids the influence of external conditions on temperature detection due to its excellent accuracy, remote detection and reversible luminescence [15-17]. Importantly, the influence of fluorescence loss and excited state fluctuation on FIR technology is weak. Compared with fluorescence lifetime temperature measurement technology, FIR is more adaptable to strong magnetic and high temperature environments [18-20]. However, the appropriate energy difference between the activated ions (200-2000 cm^{-1}) is the key factor to realize FIR technology. Therefore, developing efficient luminescent materials based on FIR technology is a challenging task.

Researchers focus on the development of double activated ions doped luminescent materials based on FIR technology. For example, Huang et al. obtained $La_2MoO_6:Yb^{3+}/Er^{3+}$ phosphor with excellent performance in temperature measurement by adjusting the cross relaxation characteristics between activated ions [21]. Zhou et al. synthesized $NaLaMgWO_6:Mn^{4+}$, Eu^{3+} phosphor. The temperature detection range is 303-523 K, and the maximum FIR is 0.86% K^{-1} [22]. Li et al. synthesized $CaMoO_4:Tb^{3+}$,

Eu^{3+} phosphor with high sensitive temperature detection performance by precipitation method [23]. Luminescent materials based on FIR technology show excellent performance in optical temperature detection. However, double red activator Sm^{3+}/Mn^{4+} co-doped red phosphor is poorly studied and rarely reported. Furthermore, it is reasonable to study inorganic luminescent materials with double red emission centers applied in the field of plant growth lighting.

Due to the complex energy level of 4f electron layer, Sm^{3+} ions present narrowband emission ($^4G_{5/2}\rightarrow{}^4H_{7/2}$, $^4G_{5/2}\rightarrow{}^4H_{5/2}$, $^4G_{5/2}\rightarrow{}^4H_{9/2}$, $^4G_{5/2}\rightarrow{}^4H_{11/2}$) in orange-red region [24, 25]. By comparison, the $3d^3$ energy level of Mn^{4+} at the center of octahedron is split into triple degenerate state (t_{2g}) and double degenerate state (e_g). Therefore, Mn^{4+} has broadband emission in the red light region. Hopefully, the valence charge transfer state between metal ions provides a novel quenching path for the crossing of excited state and ground state energy levels, which plays an important role in novel temperature monitoring. Importantly, both rare earth ions Sm^{3+} and transition metal ions Mn^{4+} with different temperature dependence can be excited by near ultraviolet (UV) and partial blue light. Therefore, Sm^{3+} and Mn^{4+} co-doped temperature sensing materials are expected to realize FIR technology. In addition, the emission areas of Sm^{3+} and Mn^{4+} ions cover the orange-red, dark-red and far-red light, which match the absorption of phytochromes P_R (660 nm) and P_{FR} (730 nm) [26-28]. Our previous work has proved that stable double perovskites Sr_2GdTaO_6 (SGTO) is a suitable host for Mn^{4+}-doped [30]. Therefore, we firmly believe that Sm^{3+}-Mn^{4+} co-doped SGTO

phosphor is expected to achieve optical temperature sensing and plant growth lighting multifunctional applications.

In this work, a series of novel SGTO:$Sm^{3+}$and SGTO:Sm^{3+}, Mn^{4+} phosphors were synthesized by high-temperature solid-state method. SGTO as a host provides suitable substitution sites for Sm^{3+} and Mn^{4+} ions, where Sm^{3+} and Mn^{4+} ions replace Gd^{3+} sites and Ta^{5+} sites, respectively. The elemental composition, morphology, luminescence mechanism and thermal stability of the materials were studied. As a result, SGTO:$Sm^{3+}$and SGTO:Sm^{3+}, Mn^{4+} phosphors are expected to play an important role in the field of plant growth lighting and optical temperature sensing.

2. Experimental Section

2.1. Sample preparation

The experimental drugs, $SrCO_3$ (99.99%), Gd_2O_3 (99.99%), Sm_2O_3 (99.99%), MnO_2 (99.99%) and Ta_2O_5 (99.99%) were purchased from Aladdin Reagents Co., Ltd. A series Sm^{3+} doped and Sm^{3+}/Mn^{4+} co-doped SGTO red phosphors were synthesized by high-temperature solid-state reaction. The above experimental drugs were weighed accurately according to the ratio of the target compounds. All raw materials were poured into the ball mill tanks, with anhydrous ethanol and ZrO_2 ball as the medium. The ball mill tanks were fixed in the ball mill, and the powders were dried in the oven after 12 h of high-speed operation. The powders were first calcined at 750 °C for 6 h to decompose carbonate. Then the powders were calcined at 1350 °C for 8 h. The caked

samples were broken into powder for subsequent testing.

2.2. Measurement and characterization

The phase of sample was collected by DX-2700B model X-ray diffractometer (XRD, Cu, Kα, λ=0.154178 nm). The morphology, microstructure and composition were observed by high resolution scanning electron microscope (SEM, Hitachi SU-5000), energy dispersive X-ray spectroscopy (EDS) and X-ray photoelectron spectrometer (XPS, ESCALAB). The light absorption property was tested by UV-Vis spectrometer (UV-2450PC, Shimadzu), $BaSO_4$ powder as the reference material. Photoluminescence property was tested by fluorescence spectrometer (Hitachi F-7000, 450W Xi). The thermal stability was tested by the same fluorescence spectrometer with a temperature control system.

3 Results and discussion

Fig.1 (a) shows the crystal structure of SGTO. The spatial configuration of SGTO double perovskites material belongs to monoclinic crystal system with the space group $P2_1/n$ [29]. Cell parameters are as follows, *a*: 5.8380(2) Å, *b*: 5.9165(4) Å, *c*: 8.2989(2) Å, *β*: 90.125(1)°[30]. Many studies have shown that atomic substitution is related to the ionic radius and coordination number (CN). Ions substitution occurs easily when ionic radius difference is less than 30%. Table.1 shows the radius deviation between the radius of Sm^{3+} ions and Ta^{5+}, Sr^{2+}, and Gd^{3+} ions in the host (SGTO). The CN of Ta^{5+}, Sr^{2+} and Gd^{3+} in the host are all 6. All ions have the possibility of being substituted. R_r is the percentage difference of radius, which is used to evaluate the radius difference

between Sm^{3+} ion and cations. Formula (1) is as follows [33]:

$$R_r = 100\% \times \frac{R_h(CN) - R_d(CN)}{R_h(CN)} \quad \text{.....(1)}$$

where, R_h (CN) and R_d (CN) represent the radius of the ions in the host and the radius of the Sm^{3+} ion, respectively. It is found that the radius of Sm^{3+} (0.96 Å, CN=6) and Gd^{3+} (0.94 Å, CN=6) are very similar under the same conditions. Besides, the possibility of ions substitution can also be determined by C/IR. C/IR represents the ratio of charge to radius. The data show that the ionic radius of Sm^{3+} ion and C/IR are similar to Gd^{3+} ions, because they belong to lanthanide elements. Therefore, it can be inferred that Sm^{3+} preferentially replaces Gd^{3+}. Fig.1 (b) shows the XRD patterns of SGTO:$x$$Sm^{3+}$ phosphors (x=0, 0.03, 0.05, 0.075, 0.1, 0.125, 0.15). Compared with the standard card (PDF#47-0527, Sr_2EuTaO_6), the diffraction peaks of all samples match the characteristic diffraction peaks. No impurity phase is observed even if the doping amount reaches 15%. The results show that Gd^{3+} is successfully replaced by Sm^{3+} in SGTO host.

Table 1. R_r between Sm^{3+} ion and metal cations in SGTO host.

ions	*CN*	Ions radius (Å)	*Rr* (%)	C/IR
Sm^{3+}	6	0.96	-	3.13
Ta^{5+}	6	0.64	17.19	7.81
Sr^{2+}	6	1.18	55.09	1.70
Gd^{3+}	6	0.94	43.62	3.19

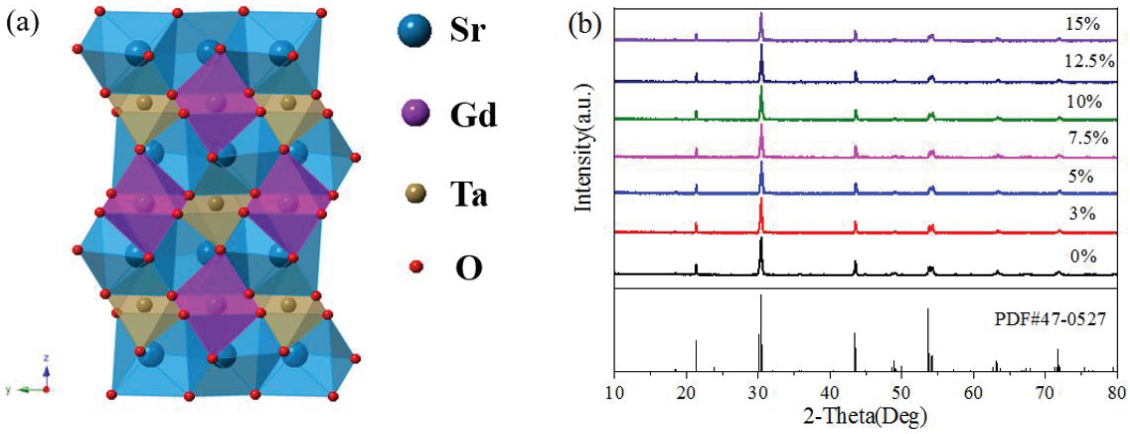

Fig. 1 (a) Crystal structure of SGTO. (b) XRD patterns of SGTO:*x*Sm^{3+}.

Fig. 2 (a) shows the SEM images of SGTO:0.075Sm^{3+}. The particles show an irregular shape and the diameter is about 1-3 μm. The EDS spectra and mapping of SGTO:0.075Sm^{3+} (Fig. 2 (b-f)) show the distribution of Sr, Gd, Ta, O, and Sm elements. Fig. 2 (g-j) describe the XPS spectra of SGTO:0.075Sm^{3+} phosphor. The characteristic combination of Sr^{2+} and Gd^{3+} can be detected, the peaks 147.7 and 141.6 eV can be attributed to $Gd4d_{3/2}$ and $Gd4d_{5/2}$, respectively, the peaks 134.4 and 132.9 eV are attributed to $Sr3d_{3/2}$ and $Sr3d_{5/2}$, respectively. Beside, $Ta4f_{5/2}$ and $Ta4f_{7/2}$ with low binding energy are found at 27.2 eV and 25.3 eV, respectively. Importantly, Sm^{3+} ions were detected, $Sm3d_{3/2}$ (1109.6 eV) and $Sm3d_{5/2}$ (1083.1 eV), which strongly proves that Sm^{3+} ions are successfully doped into SGTO host.

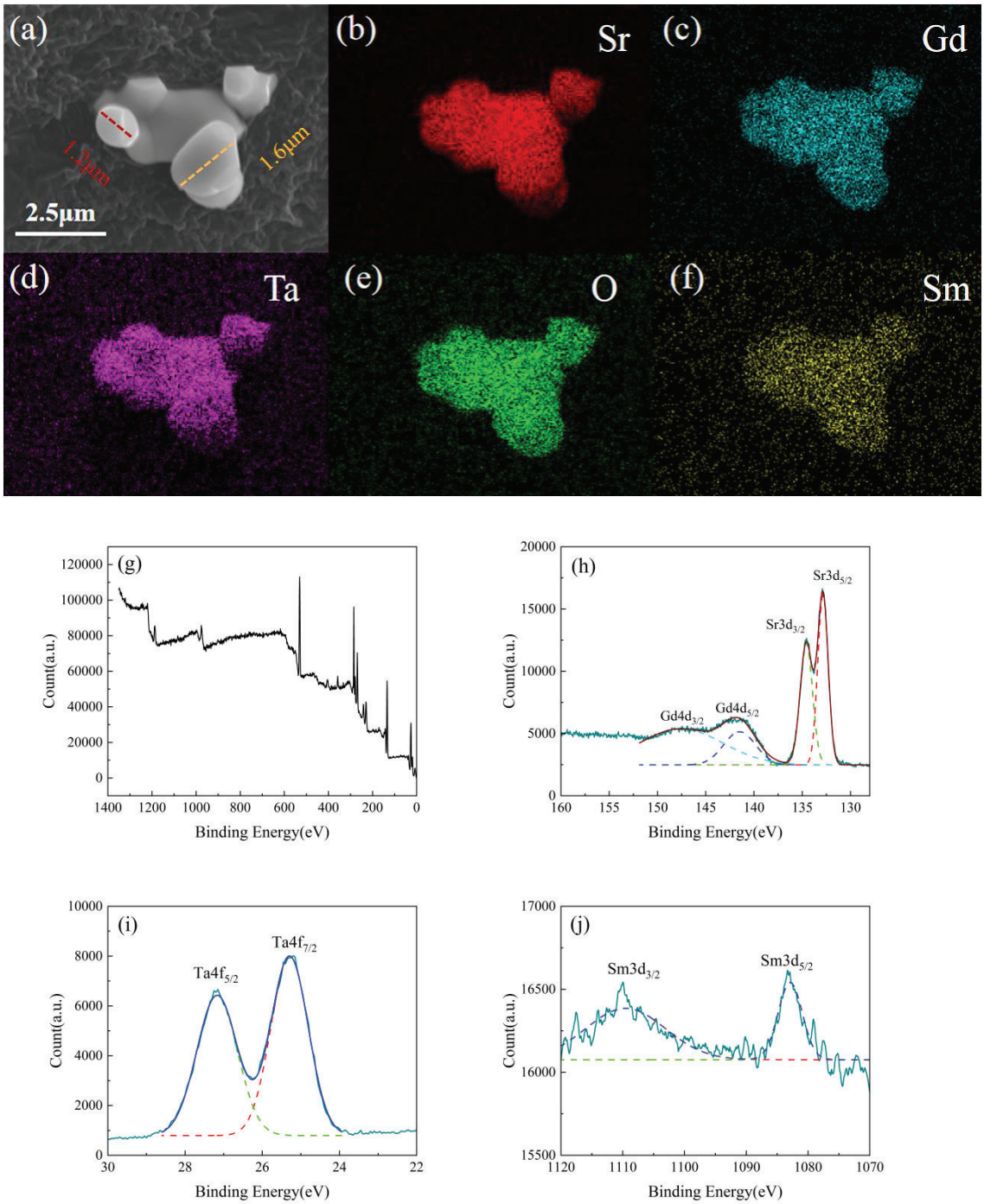

Fig. 2 (a) SEM image of SGTO:0.075Sm^{3+}. Element distributions: (b) Sr, (c) Gd, (d) Ta, (e) O, (f) Sm. XPS spectra of (g) SGTO:0.075Sm^{3+}, (h) Sr3d and Gd4d, (i) Ta4f, (j) Sm3d.

Fig. 3 (a) shows the PLE spectrum of SGTO:0.075Sm^{3+} phosphor (λ_{em}=606 nm). The PLE spectrum is mainly contributed by the $^6H_{5/2}\rightarrow{}^4F_{7/2}$ (408 nm) energy level leap.

Several other absorption peaks: $^6H_{5/2}\rightarrow{}^4I_{11/2}$ (468 nm) , $^6H_{5/2}\rightarrow{}^6P_{7/2}$,$^4P_{7/2}$ (419 nm) , $^6H_{5/2}\rightarrow{}^4I_{9/2}$ (483 nm), $^6H_{5/2}\rightarrow{}^4L_{15/2}$ (383 nm) , $^6H_{5/2}\rightarrow{}^6P_{5/2}$ (437 nm), $^6H_{5/2}\rightarrow{}^4I_{13/2}$ (450 nm), $^6H_{5/2}\rightarrow{}^4D_{3/2}$ (358 nm). Fig. 3 (b) shows the PL spectrum of SGTO:0.075Sm^{3+} (λ_{em}=408 nm). The PL spectrum is mainly composed of four parts (sort by intensity): $^4G_{5/2}\rightarrow{}^4H_{7/2}$, $^4G_{5/2}\rightarrow{}^4H_{5/2}$, $^4G_{5/2}\rightarrow{}^4H_{9/2}$, $^4G_{5/2}\rightarrow{}^4H_{11/2}$. Among them, peak splitting occurs in $^4G_{5/2}\rightarrow{}^4H_{7/2}$ and $^4G_{5/2}\rightarrow{}^4H_{5/2}$, this indicates that the crystal field splits the partially excited state energy levels of Sm^{3+}[34-36]. Fig. 3 (c) and (d) show the PL spectra of samples with different Sm^{3+} concentration and the PL intensity change trend, respectively. Beyond all doubt, SGTO:0.075Sm^{3+} exhibits the strongest PL intensity, and the concentration quenching occurs when the doping amount is greater than 7.5%. A large number of activated ions shorten the distance between each other, R_c is defined as the critical distance leading to concentration quenching and can be calculated by formula (2) [37]:

$$R_c=2\left(\frac{3V}{4\pi x_c N}\right)^{\frac{1}{3}} \quad \text{(2)}$$

where, V is the volume of a cell, x_c is the doping concentration at quenching, N is coordination number. Here, V = 286.65 $Å^3$, x_c = 0.075, N = 4, we calculate R_c=6.1 Å. Obviously, R_c is greater than 5 Å, which inferred that the quenching mechanism of SGTO: Sm^{3+} is multipolar interaction, as shown in formula (3) [37]:

$$I/x = K\left[1+\beta(x)^{\theta/3}\right]^{-1} \quad \text{(3)}$$

where, $\boldsymbol{I}$ is PL intensity at optimal doping concentration, $\boldsymbol{x}$ is optimal doping concentration, K and β are constants. The tangent obtained in Fig. 3 (e) is the value of

θ/3, therefore, θ = 3.651 approach 6, which correspond to dipole-dipole (*d*-*d*) interaction. Fig. 3 (f) depicts the UV-Vis DR spectra of SGTO:xSm^{3+} phosphors. The absorption part is mainly composed of two parts. The valley in the far UV region is attributed to the energy absorbed by the SGTO host, and the NUV absorption attribution and electronic transition of Sm^{3+}. Fig. 4 draws the calculated Commission Internationale de l' Eclairage (CIE) diagram of SGTO:xSm^{3+}. The chromaticity coordinates is calculated to be (0.491, 0.499), (0.492, 0.498), (0.505, 0.472), (0.503, 0.478), (0.503, 0.479) and (0.499, 0.482), corresponding to SGTO:xSm^{3+} (x=0.03, 0.05, 0.075, 0.01, 0.125 and 0.15).

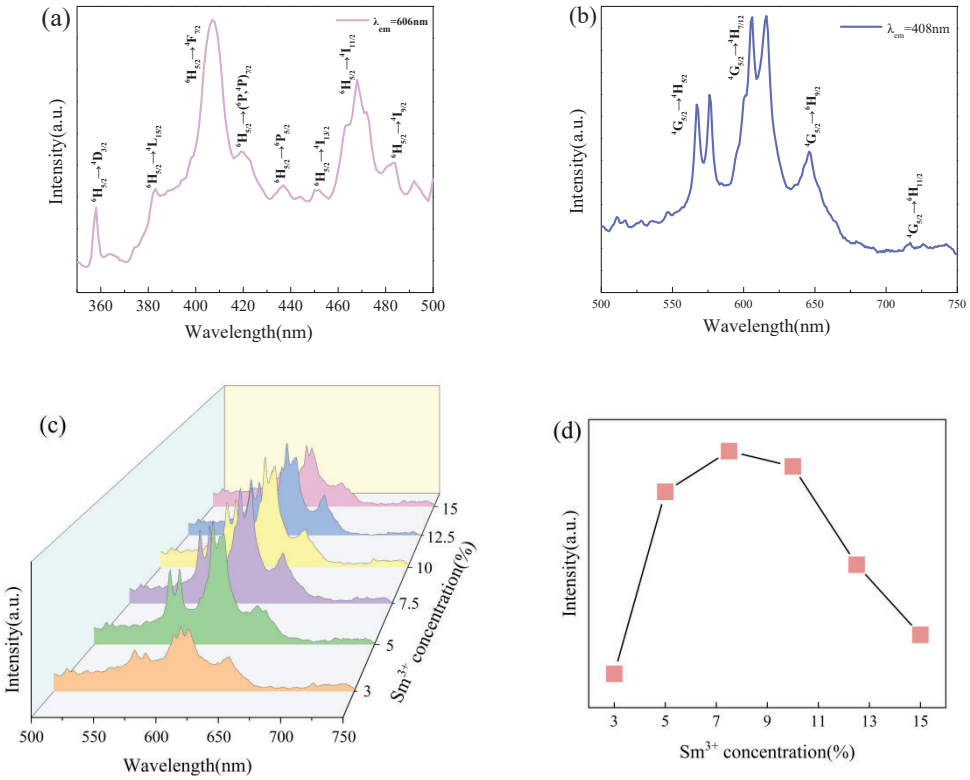

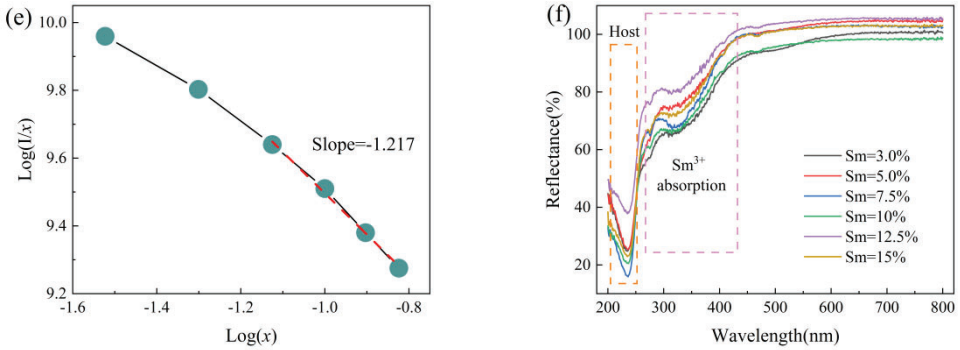

Fig. 3 (a) PLE spectrum and (b) PL spectrum of SGTO:0.075Sm^{3+} phosphor. (c) PL spectra of SGTO:*x*Sm^{3+} phosphors. (d) PL intensity of SGTO:*x*Sm^{3+} phosphors. (e) Log(*x*) dependent Log(I/*x*) and fitting curve. (f) UV-Vis DRS of SGTO:*x*Sm^{3+} phosphors.

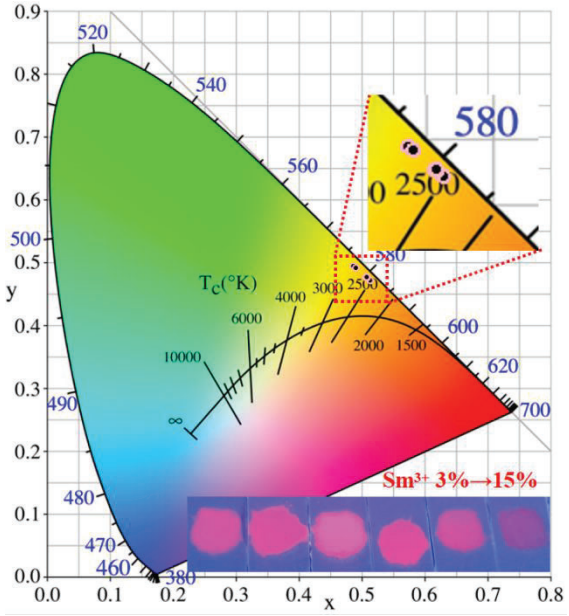

Fig. 4 CIE of SGTO:*x*Sm^{3+}, inset: photos of SGTO:*x*Sm^{3+} under 365 nm illumination.

Fig. 5 (a) shows the PL intensity dependent temperature curves, temperature detection range from 298 to 573 K. The emission peak is mainly composed of three parts, which is consistent with the previous emission spectra analysis. The PL intensity decreases as temperature rises indicates that thermal quenching phenomenon occurs. In order to better understand the thermodynamic properties of the sample, the Arrhenius

equation is used to calculate the thermal activation energy (E_a)[38]:

$$I(T) = \frac{I_0}{1 + c\exp(-E_a / KT)} \quad \text{.....(4)}$$

where, I_0 and $I(T)$ are the PL intensity at room temperature and temperature (T), respectively. K is Boltzmann constant and **c** is constant. After logarithmic deformation of the formula, 10000/T dependent Ln(I_0/I-1) and fitting curve are shown in Fig. 5 (b), the slope =-0.251 means E_a=0.217 eV. This result shows that the excited electrons in the thermal quenching process must at least cross 0.217 eV energy gap, and then return to the ground state in the form of non radiative transition.

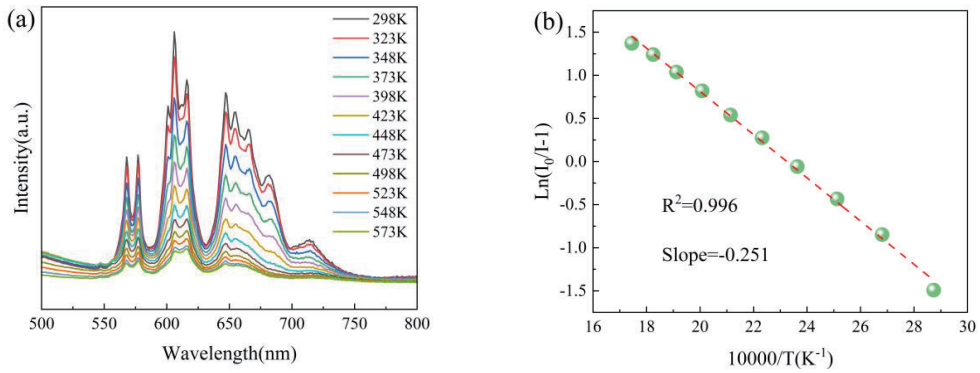

Fig. 5 (a) PL spectra of SGTO:0.075Sm^{3+} depend on temperature. (b) 10000/T dependent Ln(I_0/I-1) and fitting curve.

Our previous work has proved that Mn^{4+} ions enter SGTO host after replacing Ta^{5+} [30]. Based on the successful synthesis of SGTO:Sm^{3+}, therefor, Sm^{3+} and Mn^{4+} double red activators co-activated SGTO were further studied. Fig. 6 (a) shows the XRD patterns of SGTO:0.075Sm^{3+}, $x$$Mn^{4+}$ (x=0.001, 0.002, 0.003, 0.005, 0.007, 0.009). The strongest emission peak of SGTO:Mn^{4+} is 652 nm. Therefore, 606 nm and 652 nm are selected to monitor excitation spectra, respectively, as shown in Fig. 6 (b). The

excitation spectrum shows the characteristic excitation peaks of Sm^{3+} under 606 nm monitoring, while the spectrum is mainly the excitation peak of Mn^{4+} under 652 nm monitoring, supplemented by Sm^{3+} peaks. The photoluminescence excitation (PLE) spectra of the samples exhibited broadband absorption (300-550 nm), which is attributed to Mn^{4+}: $^4A_2 \rightarrow {}^4T_1$, $^4A_2 \rightarrow {}^2T_2$ and $^4A_2 \rightarrow {}^4T_2$ transitions (Deconvolution can be referred to[30]). In order to balance the emission of Sm^{3+} and Mn^{4+}, 408 nm is selected as the excitation wavelength. Fig. 6 (c) shows the PL spectra of SGTO:0.075Sm^{3+}, $x$$Mn^{4+}$ phosphors. All emission peaks have the same shape but different intensity. Obviously, the emission peaks of Sm^{3+} and Mn^{4+} coexist in the PL spectra. The PL intensity of SGTO:0.075Sm^{3+}, $x$$Mn^{4+}$ is counted by integral. It is found that when the Mn^{4+} doping concentration is 0.3 mol%, the PL intensity of the phosphor reaches the extreme value, as shown in Fig. 6 (d). Therefore, SGTO:0.075Sm^{3+}, 0.003Mn^{4+} phosphor is used for related research of plant growth lighting and optical temperature sensing.

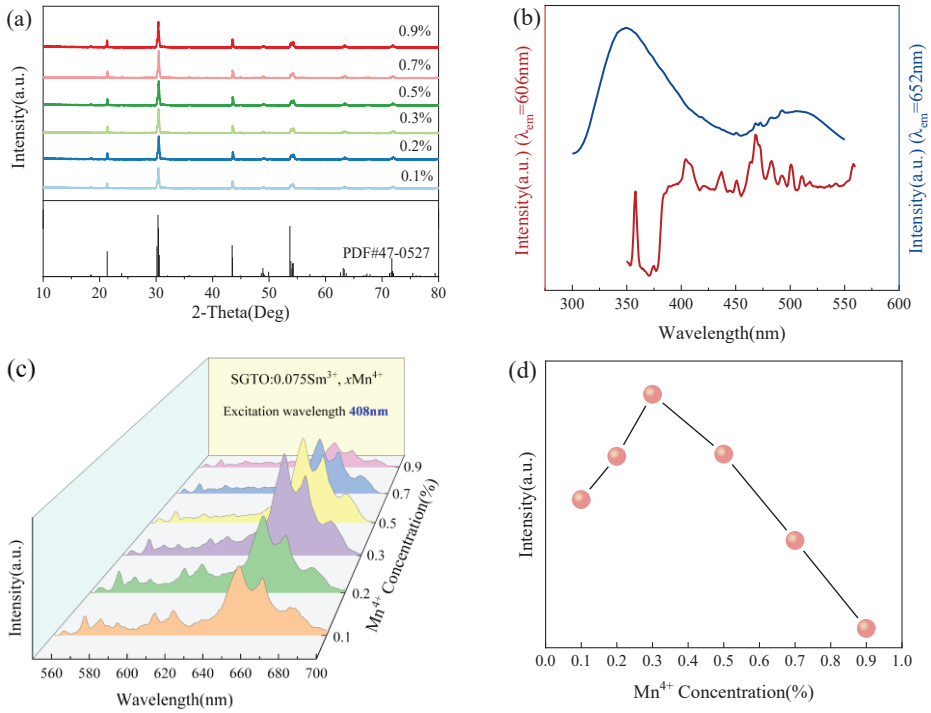

Fig. 6 (a) XRD patterns of SGTO:0.075Sm^{3+}, xMn^{4+}. (b) PLE spectra of SGTO:0.075Sm^{3+}, 0.003Mn^{4+} (λ_{em}=606 nm and 652 nm). (c) PL spectra of SGTO:0.075Sm^{3+}, xMn^{4+}. (d) PL intensity of SGTO:0.075Sm^{3+}, xMn^{4+}.

Related literature reports that phytochromes P_R and P_{FR} in plant are sensitive to red light[27-29]. The emission spectra of SGTO:0.075Sm^{3+} and SGTO:0.075Sm^{3+}, 0.003Mn^{4+} and the absorption spectra of P_R and P_{FR} are compared, as shown in Fig. 7 (a) and (b). The PL spectrum of SGTO:0.075Sm^{3+} ($^4G_{5/2}\rightarrow{}^6H_{9/2}$, $^4G_{5/2}\rightarrow{}^4H_{7/2}$, $^4G_{5/2}\rightarrow{}^4H_{5/2}$, $^4G_{5/2}\rightarrow{}^4H_{11/2}$) covers the part of the P_R absorption spectra. By comparison, the emission peaks of Sm^{3+} and Mn^{4+} co-doped phosphors match well with phytochromes P_R and P_{FR}. Benefit from the emission of Sm^{3+} ions, the problem of insufficient P_R irradiation is effectively compensated. Therefore, SGTO:0.075Sm^{3+}, 0.003Mn^{4+} with broad emission is more suitable for plant lighting.

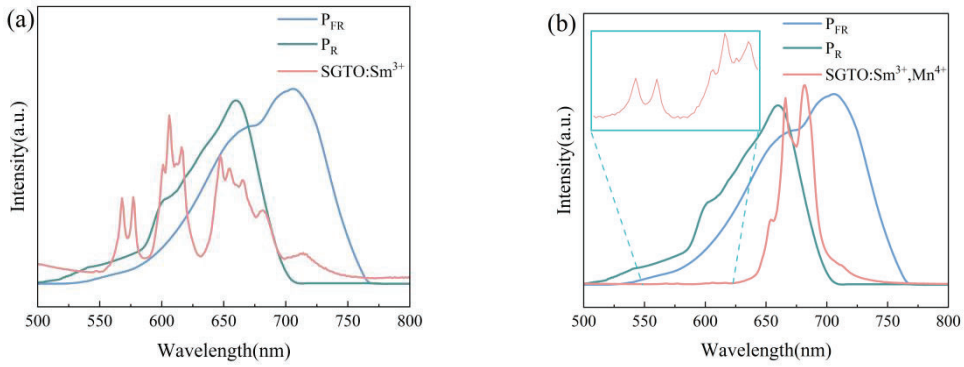

Fig. 7 Absorption spectra of phytochromes P_R and P_{FR} and PL spectrum of (a) SGTO:0.075Sm^{3+}, (b) SGTO:0.075Sm^{3+}, 0.003Mn^{4+}.

Many studies have shown that transition ions and trivalent rare earth ions usually have different temperature dependence Therefore, the application of Sm^{3+} and Mn^{4+} in the field of temperature sensing is explored by FIR technique. As shown in Fig. 8 (a), the variable temperature spectra of SGTO:0.075Sm^{3+}, 0.003Mn^{4+} show that the increase of temperature leads to the thermal quenching of the material. However, the quenching of Sm^{3+} and Mn^{4+} are different at the same temperature. When the temperature is close to room temperature, the emission of Mn^{4+} is absolutely dominant, and the PL intensity of Mn^{4+} ions decreases after the temperature increases, as shown in Fig. 8 (b). In order to further study the temperature detection ability of the material, FIR can be fitted exponentially by the following formula [15]:

$$FIR = \frac{I_{Sm}(T)}{I_{Mn}(T)} = \frac{I_{0,}Mn^{4+}}{I_{0,}Sm^{3+}} \frac{1 + A_{Sm^{3+}} \exp(-\frac{E_{Sm^{3+}}}{K_B T})}{1 + A_{Mn^{4+}} \exp(-\frac{E_{Mn^{4+}}}{K_B T})} \approx B + C \bullet \exp(\frac{-\Delta E}{K_B T}) \quad \text{..... (5)}$$

where, B and C are constants, T is temperature, K_B is Boltzmann constant. As show in

Fig. 8 (c), FIR=24005.46 exp(-5882.35/T) +0.01 is obtained from the data points after exponential fitting, R^2=0.995 proves high fitting accuracy. Two important indicators relative sensitivity (S_r) and absolute sensitivity (S_a) are used to judge the application prospect of materials, S_r and S_a can be calculated by the following formula [39]:

$$Sa = \left| \frac{\partial FIR}{\partial T} \right| = C\exp\left(\frac{B}{T}\right) \times \frac{-B}{T^2} \quad \text{.....(6)}$$

$$Sr = 100\% \times \left| \frac{1}{FIR} \times \frac{\partial FIR}{\partial T} \right| = \frac{C\exp\left(\frac{B}{T}\right)}{B + C\exp\left(\frac{B}{T}\right)} \times \frac{(-B)}{T^2} \times 100\% \quad \text{.....(7)}$$

The calculated results are plotted in Fig. 8 (d). Obviously, the value of S_r decreases monotonically, but the value of S_a increases monotonically. The maximum values of S_r and S_a are 2.94 K^{-1} at 298 K and 0.635 K^{-1} at 573 K, respectively. This result shows that SGTO:0.075Sm^{3+}, 0.003Mn^{4+} red phosphor has application value in the field of optical temperature sensing [47-48].

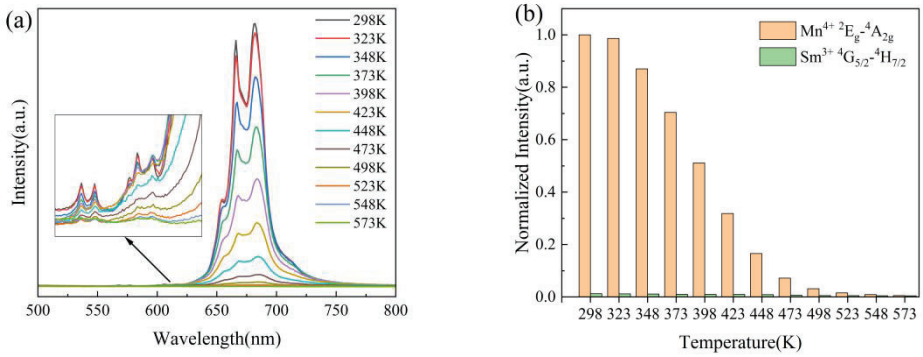

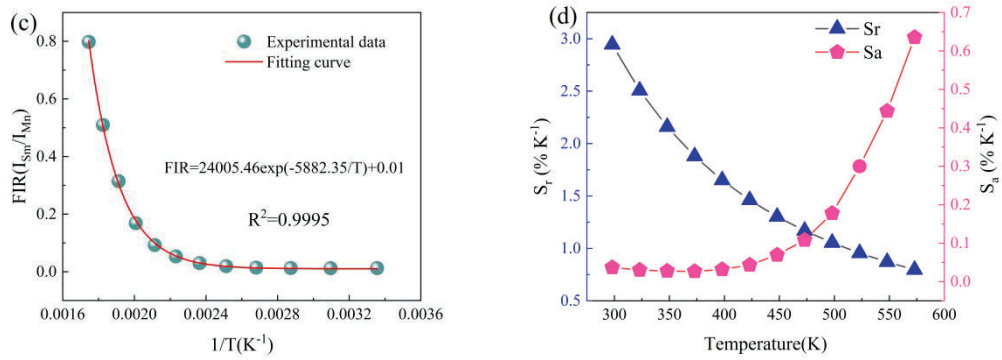

Fig. 8 (a) PL spectra of SGTO:0.075Sm^{3+}, 0.003Mn^{4+} depend on temperature. (b) The normalized PL intensities (Sm^{3+}: $^4G^{5/2}\rightarrow{}^4H_{5,7/2}$ and Mn^{4+}: $^2E_g\rightarrow{}^4A_{2g}$) at distinct temperatures. (c) Experimental measured and fitting curve of FIR temperature depend on 1/T of SGTO:0.075Sm^{3+}, 0.003Mn^{4+}. (d) $\boldsymbol{S_a}$ and $\boldsymbol{S_r}$ depend on temperatures (293-573 K).

4. Conclusions

In summary, a series of Sm^{3+} doped and Sm^{3+}-Mn^{4+} co-doped SGTO red phosphors were synthesized by high-temperature solid-phase reaction method. SGTO:0.075Sm^{3+} exhibits the maximum red emission intensity in the range (560-670 nm). The concentration quenching mechanism of Sm^{3+} in SGTO is *d-d* interaction and E_a=0.217 eV. The emission range of SGTO:0.075Sm^{3+} after introducing Mn^{4+} is mainly dark red light emission in the range from 630 to 750 nm, and the optimum doping concentration of Mn^{4+} is 0.3%. The PL spectra of SGTO:0.075Sm^{3+}, 0.003Mn^{4+} match the red light required for plant growth. The maximum value of S_r and S_a are 2.94 K^{-1} (298 K) and 0.635 K^{-1} (573 K), respectively. This work not only illustrates that SGTO:0.075Sm^{3+}, 0.003Mn^{4+} phosphors have the potential in plant growth lighting and optical temperature sensing, but also provides a model for double red activated ions

doped phosphor.

Acknowledgments

This work is supported by Ph.D. Student Research and Innovation Fund of the Fundamental Research Funds for the Central Universities (Grant No. 3072022GIP2501); Fundamental Research Funds for the Central Universities (3072022CF2506); Ministry of Science and Technology "High-end Foreign Expert Introduction Program"(G2022180002); National Natural Science Foundation of China (11574061, 62065001); Natural Science Foundation of Heilongjiang Province (LH2021F019); Natural Science Foundation of Zhejiang Province of China (LGG20E040001).

References

[1] S.A. Wade, S.F. Collins, G.W. Baxter, Fluorescence intensity ratio technique for optical fiber point temperature sensing, J. Appl. Phys. 94 (2003) 4743-4756.

[2] Y. Song, N. Guo, J. Li, R. Ouyang, Y. Miao, B. Shao, Photoluminescence and temperature sensing of lanthanide Eu^{3+} and transition metal Mn^{4+} dual-doped antimoniate phosphor through site-beneficial occupation, Ceram. Int. 46 (2020) 22164-22170.

[3] X.D. Wang, O.S. Wolfbeis, R.J. Meier, Luminescent probes and sensors for temperature, Chem. Soc. Rev. 42 (2013) 7834-7869.

[4] H. Zhang, Z.Y. Gao, G.G. Li, Y.L. Zhu, S.Q. Liu, K. Li, Y.J. Liang, A ratiometric optical thermometer with multi-color emission and high sensitivity based on double

perovskite $LaMg_{0.402}Nb_{0.598}O_3$: Pr^{3+} thermochromic phosphors, Chem. Eng. J. 380 (2020) 122491.

[5] K. Li, M. Shang, H. Lian, J. Lin, Recent development in phosphors with different emitting colors via energy transfer, J. Mater. Chem. C. 4 (2016) 5507-5530.

[6] C.C. Lin, A. Meijerink, R.S. Liu, Critical red components for next-generation white LEDs, J. Phys. Chem. Lett. 7 (2016) 495-503.

[7] D. Chen, S. Liu, Y. Zhou, Z. Wan, P. Huang, Z. Ji, Dual-activator luminescence of RE/TM: $Y_3Al_5O_{12}$ (RE = Eu^{3+}, Tb^3, Dy^{3+}; TM = Mn^{4+}, Cr^{3+}) phosphors for self-referencing optical thermometry, J. Mater. Chem. C. 4 (2016) 9044-9051.

[8] W. Xu, Q. Song, L. Zheng, Z. Zhang, W. Cao, Optical temperature sensing based on the near-infrared emissions from Nd^{3+} /Yb^{3+} codoped $CaWO_4$, Opt. Lett. 39 (2014) 4635-4638.

[9] S. Pimputkar, J.S. Speck, S.P. Denbaars, S. Nakamura, Prospects for LED lighting, Nat. Photon. 3 (2009) 180-182.

[10] Y.T. Ren, Z.W. Yang, M.J. Li, J.F. Ruan, J.Y. Zhao, J.B. Qiu, Z.G. Song, D.C. Zhou, Reversible upconversion luminescence modification based on photochromism in $BaMgSiO_4$: Yb^{3+}, Tb^{3+} ceramics for anti-counterfeiting applications, Adv. Optical. Mater. 7 (2019) 1900213.

[11] S.L. Shinde, K.K. Nanda, Wide-range temperature sensing using highly sensitive green-luminescent ZnO and PMMA-ZnO film as a non-contact optical probe, Angew. Chem. 125 (2013) 11535-11538.

[12] Y. Gao, F. Huang, H. Lin, J.J. Zhou, J. Xu, Y.S. Wang, A novel optical thermometry strategy based on diverse thermal response from two intervalence charge transfer states, Adv. Funct. Mater. 26 (2016) 3139-3145.

[13] X.Y. Yun, J. Zhou, Y.H. Zhu, X. Li, S. Liu, D.H. Xu. A potentially multifunctional double-perovskite Sr_2ScTaO_6: Mn^{4+}, Eu^{3+} phosphor for optical temperature sensing and indoor plant growth lighting, J. Lumin. 244 (2022) 118724.

[14] C.D.S. Brites, K. Fiaczyk, J.F.C.B. Ramalho, M. Sójka, L.D. Carlos, E. Zych, Widening the temperature range of luminescent thermometers through the intra-and interconfigurational transitions of Pr^{3+}, Adv. Opt. Mater. 6 (2018) 1701318.

[15] P. Wang, J. Mao, L. Zhao, B. Jiang, C. Xie, Y. Lin, F. Chi, M. Yin, Y. Chen, Double perovskite A_2LaNbO_6: Mn^{4+}, Eu^{3+}(A=Ba, Ca) phosphors: potential applications in optical temperature sensing, Dalton. Trans. 48 (2019) 10062-10069.

[16] Z.L. Ji, Y. Cheng, X.S. Cui, H. Lin, J. Xu, Y.S. Wang, Heating-induced abnormal increase in Yb^{3+} excited state lifetime and its potential application in lifetime luminescence nanothermometry, Inorg. Chem. Front. 6 (2019) 110-116.

[17] A. Pandey, V.K. Rai, Optical thermometry using FIR of two close lying levels of different ions in Y_2O_3:Ho^{3+}-Tm^{3+}-Yb^{3+}phosphor, Appl. Phys. B. 113 (2013) 221-225.

[18] Y.F. Wu, H. Suo, X.Q. Zhao, Z.W. Zhou, C.F. Guo, Self-calibrated optical thermo-meter $LuNbO_4$:Pr^{3+}/Tb^{3+} based on intervalence charge transfer transitions, Inorg. Chem. Front. 5 (2018) 2456-2461.

[19] S.K. Singh, K. Kumar, S.B. Rai, Er^{3+}/Yb^{3+} codoped Gd_2O_3 nano-phosphor for

optical thermometry, Sens. Actuator. A. 149 (2009) 16-20.

[20] H. Kusama, O.J. Sovers, T. Yoshioka, Line Shift method for phosphor temperature measurements, Jpn. J. Appl. Phys. 15 (1976) 2349-2358.

[21] F. Huang, T. Yang, S.X. Wang, L. Lin, T. Hu, D.Q. Chen, Temperature sensitive cross relaxation between Er^{3+} ions in laminated hosts: a novel mechanism for thermo-chromic upconversion and high performance thermometry, J. Mater. Chem. C. 6 (2018) 12364-12370.

[22] Z. Long, S. Xiao, X. Yang, Mn^{4+}, Eu^{3+} Co-doped $K_{0.3}La_{1.233}MgWO_6$: a potentially multifunctional luminescent material, ACS. Appl. Electron. Mater. 2 (2020) 3889-3897.

[23] S.D. Li, Q.Y. Meng, S.C. Lü, W.J. Sun, Study on optical temperature sensing properties of Tb^{3+}, Eu^{3+} co-doped $CaMoO_4$ phosphor, J. Lumin. 200 (2018) 103-110.

[24] B.J. Han, X.H. Yang, Y.H. Jiang, Z.A. Li, Y. Shen, X.Y. Chang, Jing. R, S. Gao, Highly efficient and thermally stable red emitting $CaGdMgNbO_6:Mn^{4+}$ double perovskites for indoor plant growth LEDs, Mater. Today. Commun. 31 (2022) 103809.

[25] L. Mei, H. Liu, L. Liao, Y. Zhang, R.V. Kumar, Structure and photoluminescence properties of red-emitting apatite-type phosphor $NaY_9(SiO_4)_6O_2$: Sm^{3+} with excellent quantum efficiency and thermal stability for solid-state lighting, Sci. Rep. 7 (2017) 15171.

[26] L. Shi, Y.J. Han, Z.G. Zhang, Z.X. Ji, D.C. Shi, X.Y. Geng, H. Zhang, M. Li, Z.W. Zhang, Synthesis and photoluminescence properties of novel $Ca_2LaSbO_6:Mn^{4+}$ double perovskite phosphor for plant growth LEDs, Ceram. Int. 45 (2019) 4739-4746.

[27] K.Y. Deng, Y.H. Jin, L.F. Yuan, B. Wang, H.Y. Wu, Y.H. Hu, A thermal-stable Mn^{4+}-doped far-red-emitting phosphor-converted LED for indoor plant cultivation, Mater. Today. Chem. 26 (2022) 101010.

[28] X. Geng, Y. Xie, X. Hu, X. Ouyang, S. Chen, X. Yao, J. Kong, J. Chen, J Guo, H. Wang, W. Zhou, Greatly enhanced deep-red luminescence performance of $Ca_2InSbO_6:Mn^{4+}$ phosphor via multiple optimization strategies, Mater. Today. Chem. 26 (2022) 101006.

[29] Z.J. Wu, L. Li, H. Li, L.S. Mei, W.D. Xia, Y.S. Yi, Y.B. Hua, Designing bifunctional platforms for LED devices and luminescence lifetime thermometers: a case of non-rare-earth Mn^{4+} doped tantalate phosphors, Dalton. Trans. 51 (2022) 9062.

[30] B.J. Han, X. Yang, J. Ren, L. Liu, E. Zhao, X. Zhu, J. Zhu, H. Ma, A. Li, P. Teng, Thermally stable deep-red emitting $Sr_2GdTaO_6:Mn^{4+}$ double perovskites for indoor plant growth LEDs, Mater. Today. Chem. 23 (2022) 100737.

[31] J.P. Perdew, K. Burke, M. Ernzerhof, Generalized gradient approximation made simple, Phys. Rev. Lett. 77 (1996) 3865-3868.

[32] G. Kresse, J. Furthmüller, Efficient iterative schemes for ab initio total-energy calculations using a plane-wave basis set, Phys. Rev. B. 54 (1996) 11169-11186.

[33]X. Geng, Y. Xie, S. Chen, J. Luo, S. Li, T. Wang, S. Zhao, H, Wang, B. Deng, R. Yu, W. Zhou, Enhanced local symmetry achieved zero-thermal-quenching luminescence characteristic in the $Ca_2InSbO_6:Sm^{3+}$ phosphors for w-LEDs, Chem. Eng. J. 410 (2021) 128396.

[34] Y.B. Hua, Z.H. Li, Synthesis and photoluminescence properties of novel orange-emitting Sr_2YSbO_6: Sm^{3+} phosphors for potential solid-state lighting, Inorg. Chem. Commun. 128 (2021) 108576.

[35] B.J. Han, J. Ren, P. P Teng, J. B. Zhu, Y. Shen, Z. A. Li, X. L. Zhu, X. H. Yang, Synthesis and photoluminescence properties of a novel double perovskite Ca_2LaSbO_6: Sm^{3+} phosphor for w-LEDs, Ceram. Int. 48 (2022) 971-980.

[36] R.P. Cao, W.H. Wang, Y. Ren, Synthesise, energy transfer and tunable emission properties of $Ba_2La_2ZnW_2O_{12}$: Sm^{3+} phosphors, J. Lumin. 235 (2021) 118054.

[37] G. Blasse, Energy transfer in oxidic phosphors, Phys. Lett. 28 (1968) 444-445.

[38] Q. Wu, Y. Li, Y. Wang, H. Liu, S. Ye, L. Zhao, J. Ding, J. Zhou, A novel narrow-band blue-emitting phosphor of Bi^{3+}-activated $Sr_3Lu_2Ge_3O_{12}$ based on a highly symmetrical crystal structure used for WLEDs and FEDs, J. Adv. Ceram. 401 (2020) 126130.

[39] Y.F. Wu, H. Suo, X.Q. Zhao, Z.W. Zhou, C.F. Guo, Self-calibrated optical thermometer $LuNbO_4$: Pr^{3+}/Tb^{3+} based on intervalence charge transfer transitions, Inorg. Chem. Front. 5 (2018) 2456-2461.